(Received 1 January 2026, Accepted 26 February 2026, Scheduled 27 April 2026)

Performance Evaluation of a Dual-Band H-Shaped Metamaterial Perfect Absorber with Polarization-Insensitive Characteristics for Satellite Communication Applications

Vanam C. Narasimhulu, Govardhani Immadi*, and Madhavareddy V. Narayana

Department of ECE, KLEF, Vaddeswaram, Guntur, Andhra Pradesh, India

ABSTRACT: A compact, double split-ring H-shaped resonator-based polarization-independent dual-band metamaterial microwave absorber (MMA) with an outstanding absorption efficiency was designed and analyzed for satellite communication applications. The H-shaped resonator-based unit cell was printed on an FR4 material using copper as the conducting material. Copper material was chosen for the radiating patch and the ground plane. A detailed parametric analysis was performed by tuning the geometrical parameters of the H-shaped MMA to achieve dual absorption bands with broad bandwidth and high absorptivity. The recommended H-shaped absorber exhibits dual absorption bandwidths of 710 MHz and 1630 MHz with FBWs of 22.95% and 19.35%. Furthermore, it maintains an absorptivity of greater than 90% across the entire spectrum of dual operating bands with almost perfect absorption of 99.99% at the resonant frequencies (3.17 GHz, 7.78 GHz) of each band. The MMA maintains an area of $0.09\lambda \times 0.09\lambda$. A simulated absorber model was fabricated, and the results have been tested using an Anritsu Combinational Analyzer (MS2037C) for experimental validation. The simulated and tested outcomes of the developed prototype are in strong alignment, rendering the absorber suitable for S-band and LEO and geostationary satellite uplinks/downlinks, with specific bands often at 7.145–7.235 GHz (uplink) and 8.4–8.5 GHz (downlink).

1. INTRODUCTION

Metamaterials (MTMs) are artificially designed materials that can provide various benefits, including reduced weight, low profile, ease of prototyping, compact device design, and innovative functionality. Researchers have focused on the unusual and unique properties of metamaterials for the effective control of electromagnetic (EM) waves. EM waves are integral to contemporary life, facilitating advancements in a wide range of technologies, including various types of wireless communication systems, medical imaging, and radar systems, which are effectively utilized across the microwave to optical spectrum. In recent years, metamaterials have become widely popular for designing absorbers owing to their potential to provide near-perfect absorption of electromagnetic waves, which is very challenging with traditional materials, as well as their compact, thin profile and flexible design. To detect material characteristics and thickness in microwave applications, a multiband metamaterial sensor based on a double stripe square enclosed split-ring resonator (SRR) has been developed [1]. For C, X, and Ku band antennas as well as other applications, a special swastika-shaped capacitive chiral structure with tails inductor-based near zero-refractive index capable of an ideal metamaterial absorber has been presented [2]. The resonator's special geometry allows it to exhibit exceptional insensitivity to changes in incidence angles and polarisation for both TE and TM modes [3]. A meander line with a parasitic resonator was introduced for C-band sensing applications. The measured parameters were more exposed to external dielectric layers than in the simulated environment, and the uneven samples caused the EM field propagation from the waveguide port to become more dispersed [4]. An analysis of two example indoor wireless trials at 2.47 GHz for EM wave modulation using a manufactured passive discrete RIS was given, along with a brief historical background of wave propagation control for optics and acoustics [5]. Perfect absorption in the visible light band is achieved by a dual-frequency adjustable ideal visible light metamaterial absorber based on the sub-wavelength range [6]. The suggested meta-atom and array structure were purposefully simulated, and their performance was analysed using MATLAB and Computer Simulation Technology (CST) tools in this numerical and experimental presentation of a left-handed meta-atom [7]. Gap coupling three hexagonal SRRs with electrical dimensions of $0.119\lambda \times 0.119\lambda$ make up the suggested compact metamaterial unit cell [8]. A metamaterial absorber (MMA) based on a cross-coupled interconnected SRR(CCI-SRR) was designed and analyzed for radar and satellite applications [9]. In [10], a multiband circular polarization selective (CPS) metasurface, which is a suitable absorber for the polarization conversion mechanism for biomedical applications. A complementary SRR MMA with double-negative (DNG) characteristics was utilized for C-band satellite communication applications in [11]. A metamaterial based on an epsilon-negative MMA was designed and experimentally analysed. The unit cell and its

* Corresponding author: Govardhani Immadi (govardhanee_ec@kluniversity.in).

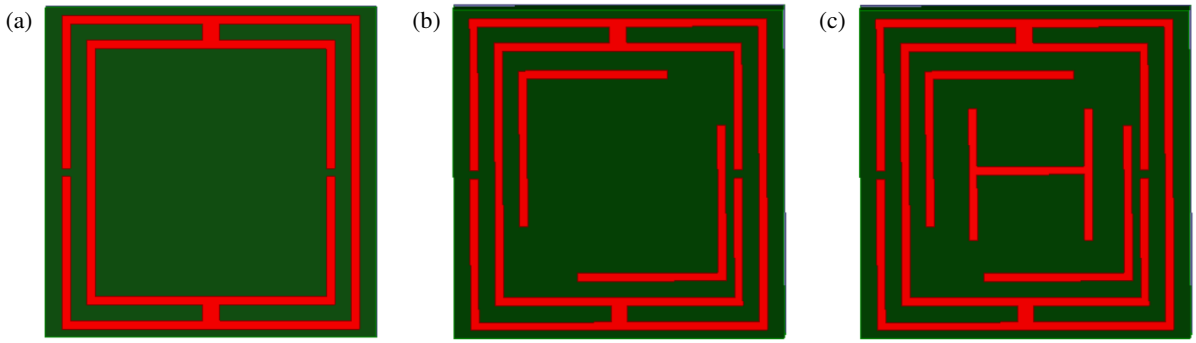

FIGURE 1. H-shaped metamaterial (MM) unit cell's evolution.

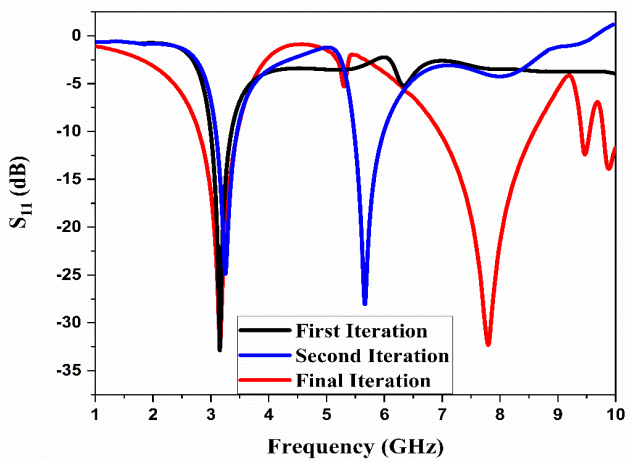

FIGURE 2. Reflection coefficients for three design iterations.

array structures have also been subjected to numerical analysis [12].

For use as a multiband absorber, a single negative metamaterial composed of an asymmetric intercoupled circular split-ring resonator is introduced [13]. In the millimeter wave frequency range, new modified negative-permeability designs with a negative refractive index were analyzed. Corner defects are added to the traditional square split ring to provide a fundamental structure [14]. This multiband MTM can be used for microwave applications, particularly for multiband antenna gain augmentation, straightforward design, compact size, high effective medium ratio (EMR), and epsilon negative property with almost negligible permeability [15]. Researchers proposed THz metamaterial absorbers by utilising different dielectric materials, such as graphene and vanadium dioxide for multiple THz applications [31–35].

This study investigates a high absorption, polarization-independent MMA for use in satellite communication applications. In the designed structure, a ring-like structure and two SRRs encircle an H-shaped resonator. The distinctive features of H-shaped MMAs include their complete absorption of 99.99% at the resonance frequencies, polarization insensitivity up to 90° incident angles, and ease of design. The refractive index of the H-shaped MMA is almost zero, and its ε and μ are negative. The CST Studio simulator was used to simulate the H-shaped MMA. The absorber is appropriate for both S-band and satellite communications, according to the close match between the simulated and measured findings.

In conclusion, this research work makes a number of important contributions.

- To obtain the best absorption for the resonant bands, the dimensions of each design parameter were modified.
- The suggested structure is appropriate for S-band (2.7 GHz–3.4 GHz) and (7 GHz–8.5 GHz) satellite communication applications. 2.7 to 3.4 GHz spectrum is also suitable for the 5G Sub-6 GHz spectrum.
- The H-shaped MTM unit cell had dimensions of ($10 \times 10\,\text{mm}^2$) and featured a simple three-layer design.
- It offers 99.99% complete absorption efficiency at both operational bands.

2. DESIGN AND ANALYSIS OF H-SHAPED METAMATERIAL ABSORBER

2.1. MTM Unit Cell Analysis

The proposed MTM unit cell underwent three design iterations, as shown in Figure 1. First, as shown in Figure 1(a), a dual-ring complementary SRR acts as a radiating element in the suggested unit cell structure. The black solid line in Figure 2 represents the first iteration unit cell, which is centered at 3.16 GHz and has an S_{11} of -33 dB. Figure 1(b) shows a rectangular loop surrounded by a complementary SRR. This loop allows the observation of an extra resonance at 5.65 GHz. As seen in Figure 2 with a blue color presentation, the second iteration unit cell resonates at 3.2 GHz and 5.65 GHz, displaying S_{11} values of -25 dB and -28 dB, respectively. Figure 1(c), which shows the structural arrangement of the last iteration step, shows that the third iteration included an H-shaped resonator. By increasing S_{11} and widening the absorption bandwidth, this H-shaped resonator improves performance. This stage's response indicates a little increase in absorption bandwidth at the -10 dB level of S_{11} by 0.7 GHz and 1.5 GHz. The red solid line represents the response of the proposed design, with a promising S_{11} value of -32 dB and a wide absorption bandwidth of 710 MHz (2.74 GHz–3.45 GHz) and 1630 MHz (6.95 GHz–8.58 GHz).

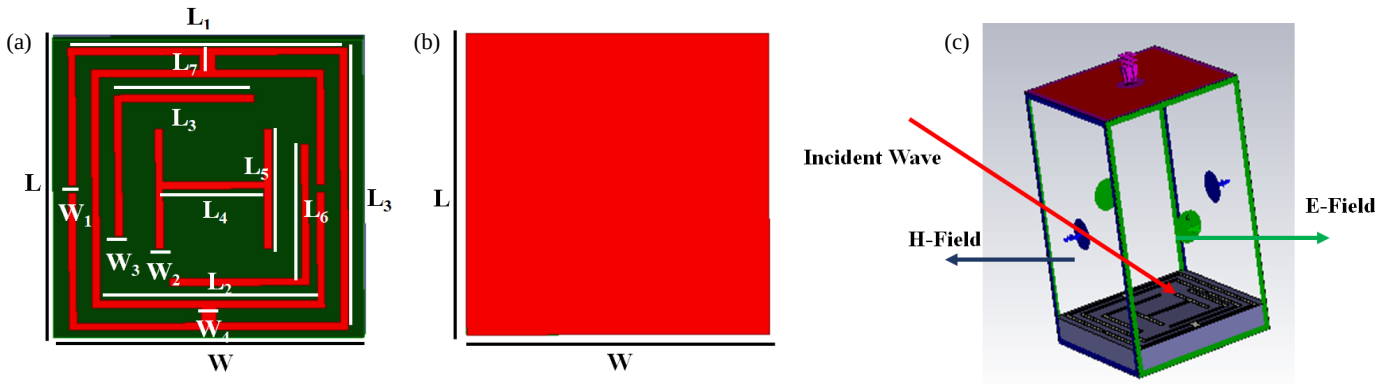

FIGURE 3. H-shaped MTM unit cell. (a) Top view. (b) Bottom view. (c) Isometric view.

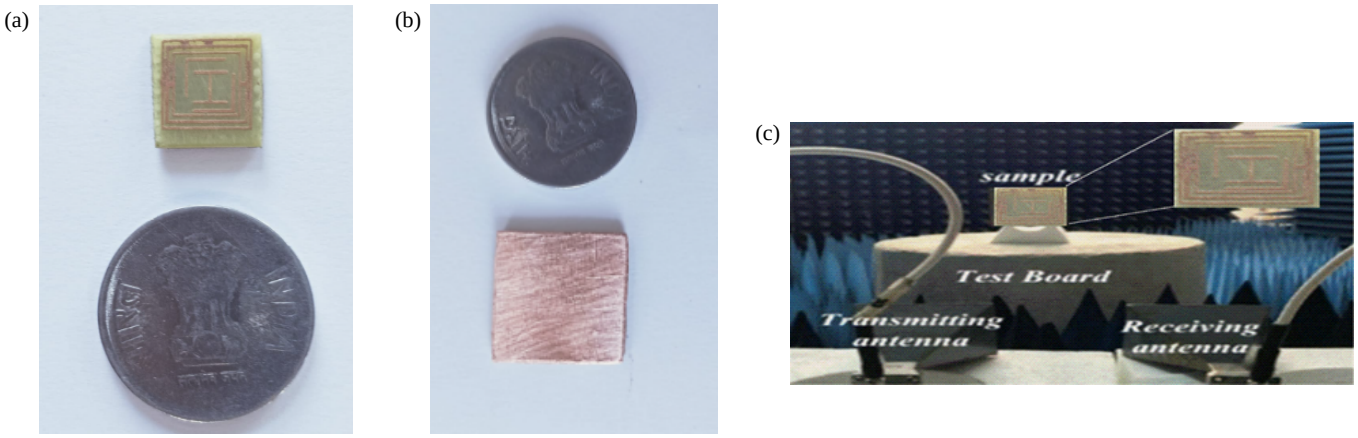

FIGURE 4. Fabricated MMA prototype and measurement setup. (a) Top surface. (b) Bottom surface. (c) Setup for measurement using Anritsu MS2037C Analyzer.

2.2. Geometry of Proposed H-Shaped Resonator-Based MMA

Figure 3 depicts the top, bottom, and isometric views of the geometrical configuration of the proposed H-shaped MMA. The design parameters have the following numerical values in millimeters: $L = W = 10$, $L_1 = 9$, $W_1 = W_2 = W_3 = 0.25$, $L_2 = 7.5$, $L_3 = L_4 = L_5 = L_6 = 4$, and $W_4 = L_7 = 0.5$. The two complementary SRRs and an H-shaped resonator encircle the proposed structure. The sub-wavelength requirements for the metamaterials are addressed by the small size of the MMA at the working frequency. Near-perfect absorptivity, compact size, polarization insensitivity, and dual broad absorption bands are just a few of the many qualities that the H-shaped MTM absorber offers. The H-shaped MMA occupies an area of $0.09\lambda \times 0.09\lambda$ and is made of FR4 material with a physical area of 10 mm $\times$ 10 mm. Because it is affordable, lightweight, and has superior electrical qualities, FR4 was selected. The copper thickness used in the design of the split-ring resonator was 0.035. Gaps and $\lambda/4$ transmission lines were used in the design of the H-shaped resonators. The properties of metamaterials, which are not found in ordinary materials, were extracted from the excited unit cell. Using the formula $2D^2/\lambda$, where λ is used to establish the boundary conditions, and D is the diameter, the E and H fields are directed towards the X and Y, respectively. The prototype MMA and its S_{11} parameter measurement setup using the Anritsu Combinational Analyzer (MS2037C) are shown in Figure 4. The measurement arrangement of the proposed metasurface is shown in Figure 4(c). Two horn antennas, one for transmitting and the other for receiving EM waves, including their experimental setup, are shown in Figure 4. These antennas are placed in the far field region and connected to an Anritsu Combinational Analyzer (MS2037C). Reflection was observed when the fabricated prototype was compared with a standard copper sheet. It shows that while the copper produces real reflection, the prototyped metasurface shows the least amount of reflection at the two resonant bands, which are 3.17 and 7.78 GHz, respectively. The absorption plot and reflection coefficient of the proposed H-shaped absorber are shown in Figure 5. CST Studio Suite 2020 is a numerical simulation tool used to acquire the desired responses of the H-shaped absorber. The proposed absorber has a near-perfect absorptivity percentage level of 99.99% and resonates at 3.17 GHz and 7.78 GHz. With an absorptivity level of 90%, it provides dual absorption bandwidths of 710 MHz and 1630 MHz with FBWs of 22.95% and 19.35% respectively.

3. METAMATERIAL (MTM) ANALYSIS OF THE ABSORBER

A detailed analysis of the metamaterial characteristics from the perspective of the recommended microwave absorber is

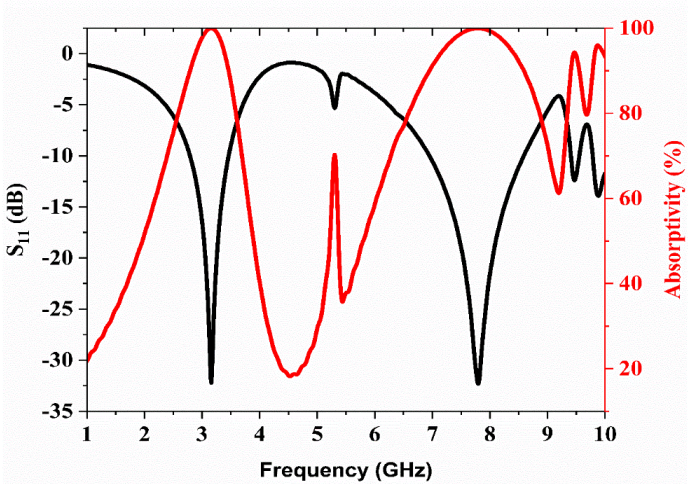

FIGURE 5. S_{11} and absorptivity responses of the recommended H-shaped absorber.

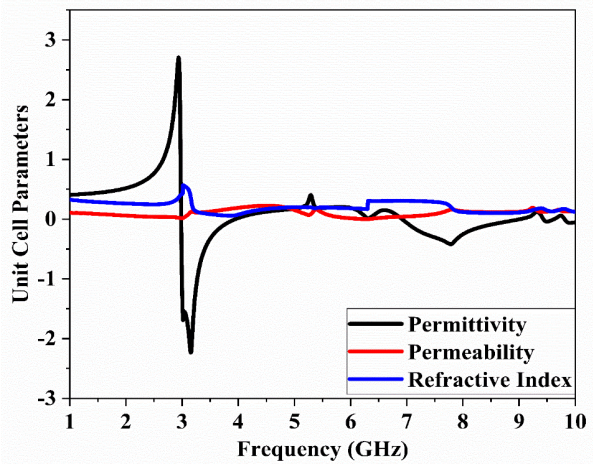

FIGURE 6. Metamaterial (MTM) unit cell properties.

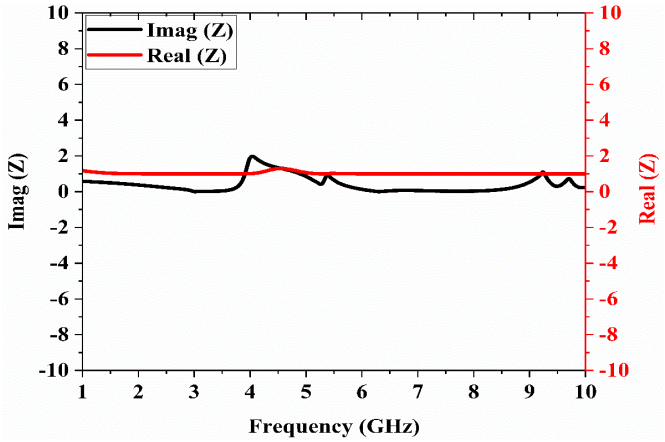

FIGURE 7. Impedance of the MTM unit cell.

explained in this section. The Nicolson-Ross-Weir (NRW) method is used for numerical validation of the MTM absorber. The NRW method is employed to extract the permeability (μ), permittivity (ε) of the metamaterial. The NRW method uses the S-parameters to derive the wave impedance (Z) and refractive index (n). Once the impedance and refractive index are calculated, the permittivity and permeability EM parameters are obtained using the subsequent mathematical Equations (1)–(4). Figure 6 explores the metamaterial properties of the MMA unit cell in terms of permeability (μ), permittivity (ε), and refractive index (n). Figure 7 represents the impedance characteristic (Z) of the H-shaped MMA [26].

$$Z = \pm\sqrt{\frac{(1+S_{11})^2 - S_{12}^2}{(1-S_{11})^2 - S_{12}^2}} \tag{1}$$

$$n = \frac{1}{K_0 d}\left\{\left[\left[\ln(e^{ink_0 d})\right]'' + 2m\pi\right] - i\left[\ln(e^{ink_0 d})\right]'\right\} \tag{2}$$

$$\varepsilon = n/Z \tag{3}$$

$$\mu = nZ \tag{4}$$

where the real and imaginary parts are indicated with the symbols ($'$) and ($''$), and impedance and refractive index are used to determine μ and ε. The EM wave is reflected, transmitted, and may even be absorbed, depending on the material characteristics. Due to this, the EM wave inside the material is attenuated. A robust retrieval technique has been utilized to extract the μ, ε, and n. According to the results depicted in Figure 6, the permittivity, refractive index, and permeability vary between negative and positive values, confirming that the unit cell has epsilon-negative properties at 3.17 GHz and 7.78 GHz. As indicated in Figure 7, at 3.17 GHz and 7.78 GHz, the real part approaches unity while the imaginary part approaches zero, confirming impedance matching with free space and resulting in minimized reflection. The material absorbs the EM wave entirely if its intrinsic impedance is equivalent to the impedance of open space.

4. ABSORPTION PHENOMENON OF THE H-SHAPED MMA

The designed MMA constitutes a split-ring resonator with a central H-shaped resonator, which is formed with recurring arrangements of metallic elements on an FR-4 substrate. The specified metallic patterned geometry of the top face, along with a complete conducting ground plane (bottom face) on the other side of the substrate, forms a promising metamaterial structure that demonstrates distinctive electromagnetic properties, which are usually absent in natural materials. When the EM waves at the specified microwave spectrum interact with the MMA, it induces surface currents on the designed metallic patterns. These currents oscillate at designated frequencies, resulting in resonance within the structure. At these resonance frequencies, the incoming microwave energy is efficiently captured and absorbed by the H-shaped MMA. The configuration of the split ring resonator and H-shaped resonators is meticulously engineered to align the impedance of the incoming EM waves with that of the MMA structure. This impedance matching reduces microwave energy reflection, facilitating more ef-

fective absorption. Concurrently, the FR4 substrate enables substantial energy dissipation inside the medium, leading to pronounced absorption and minimal transmission owing to the complete metallic ground plane at the backside. By lowering microwave energy reflection, this impedance matching promotes more efficient absorption. Due to the full metallic ground plane at the rear, the FR4 substrate simultaneously permits significant energy dissipation within the medium, resulting in significant absorption and little transmission. The dual-band absorption behavior of the proposed H-shaped metamaterial absorber originates from two distinct but electromagnetically coupled resonant modes supported by the composite metallic structure over a grounded dielectric substrate. When resonance occurs, the effective impedance of the structure satisfies (5).

$$Z_{eff} = \sqrt{\frac{\mu_{eff}}{\gamma_{eff}}} \approx Z_0 \tag{5}$$

MTM unit cell's absorption coefficient is obtained using Equations (6)–(9) [26, 27].

$$A(\omega) = 1 - |S_{11}(\omega)|^2 - |S_{21}(\omega)|^2 \tag{6}$$

where S_{21} represents the transmitted power, and S_{11} represents the reflected power. The bottom layer of the unit cell is made entirely of copper, which restricts the propagation of incident waves and leads to zero transmission ($|S_{21}(\omega)|^2 = 0$). Thus, it is possible to restructure Equation (7) such that it appears in Equation (6).

$$A(\omega) = 1 - |S_{11}(\omega)|^2 \tag{7}$$

The S-parameters represented by Equations (7) and (8), obtained from post-processing in CST Studio Suite 2020, were utilized to determine the metamaterial properties of the H-shaped MMA.

$$\text{Reflection coefficient } (S_{11}) = \frac{R_{01}(1 - e^{i2nk_0d})}{1 - R_{01}^2 e^{i2nk_0d}} \tag{8}$$

$$\text{Transmission coefficient } (S_{21}) = \frac{(1 - R_{01}^2)e^{ink_0d}}{1 - R_{01}^2 e^{i2nk_0d}} \tag{9}$$

where $R_{01} = \frac{Z-1}{Z+1}$.

Figure 8 illustrates the computed and measured absorption response of the H-shaped absorber. The conventional Short-Load-Open-Thru method was employed for calibration by connecting two cables to the analyser. The measurement of S_{11} on the copper plate was conducted initially. The H-shaped MTM unit cell was subsequently positioned at the same location, and S_{11} was measured. The actual S_{11} was ascertained by analyzing the reflected power from the absorber and the copper plate. The absorptivity result was derived from the resulting S_{11}. The results indicate the existence of dual broad absorption bands, with absorptivity exceeding 90%. The simulation and measurement findings were compatible, confirming the validity of the proposed MMA for satellite communication. Nonetheless, a minor discrepancy between the simulated and measured outcomes was observed owing to the absorber's limited dimensions and manufacturing tolerances.

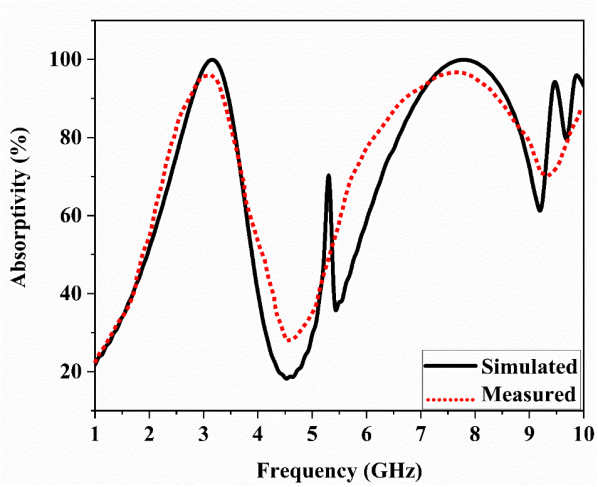

FIGURE 8. Absorptivity response of the H-shaped MTM absorber.

5. PARAMETRIC ANALYSIS OF THE H-SHAPED MMA

A parametric study of the geometrical characteristics of the H-shaped MMA usually defines the best performance of the structure. Figure 9 shows three separate graphs that show the performance of the H-shaped resonator for various length parameters (L_5) in millimeters (mm), specifically 3, 4, and 5 mm. Green solid line in these variously colored curves depicts the absorptivity (%) for $L_5 = 3$ mm, red solid line for $L_5 = 4$ mm, and black solid line for $L_5 = 5$ mm. Around 3.17 GHz and 7.78 GHz, a noticeable amount of absorption is seen. The structure exhibited the best performance for $L_5 = 4$ mm out of all the possibilities. The strip width (W_2) parameter is varied from 0.15 mm to 0.35 mm for parametric analysis, as shown in Figure 10. The absorptivity increased significantly and reached its maximum value when $W_2 = 0.25$ mm is utilised.

6. ARRAY ANALYSIS OF H-SHAPED MMA

6.1. 2 × 2 Array

The H-shaped absorber unit cell was set up in a 2 × 2 array, serving as a metasurface. Figure 13 represents the reflection coefficient that is measured across a frequency range of 3.17 and 7.78 GHz by simulating the suggested 2 × 2 unit cell structure, as depicted in Figure 11. A prototype of the 2 × 2 H-shaped MMA is shown in Figure 12. These characteristics indicate whether the metasurface transmits or reflects incident electromagnetic waves. The electromagnetic response of the metasurface changes with frequency, demonstrating an essential component of performance attributes, including resonance behavior. The design was set up in the simulation setup using a 2 × 2 array and pattern tool. To reliably extract the S parameters (S_{11}, S_{21}, etc.) and precisely model the periodic behavior, appropriate boundary conditions were developed. This configuration makes it possible to analyze the frequency-dependent response of a metasurface, which is essential for determining whether it is appropriate for uses such as absorption, beam shaping, or filtering. The proposed absorber resonates at 3.17 GHz and 7.78 GHz. It provides dual absorption bandwidths of 710 MHz and 1630 MHz with FBWs of 22.95% and 19.35%.

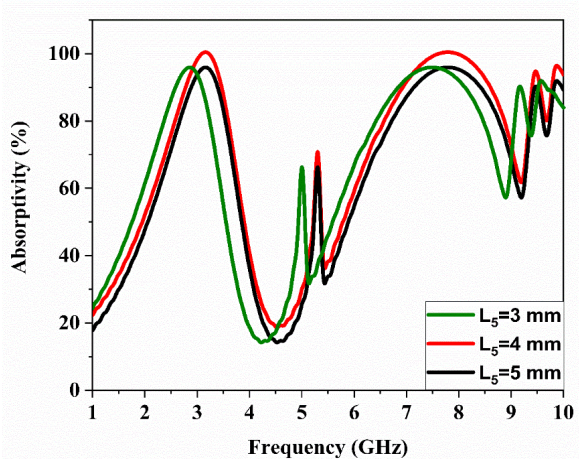

FIGURE 9. S_{11} (dB) for different lengths (L_5) of the H-shaped resonator.

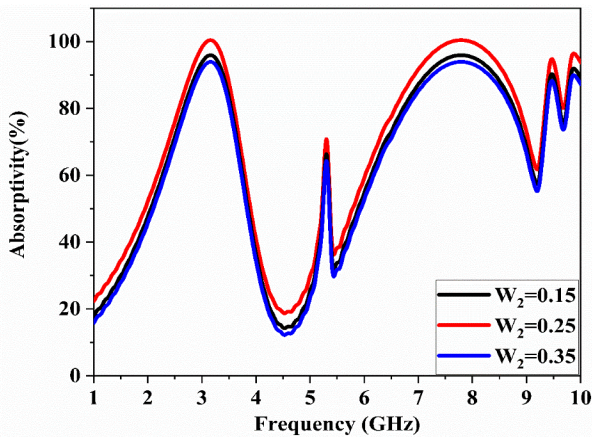

FIGURE 10. S_{11} (dB) for different widths (W_2) of the H-shaped resonator.

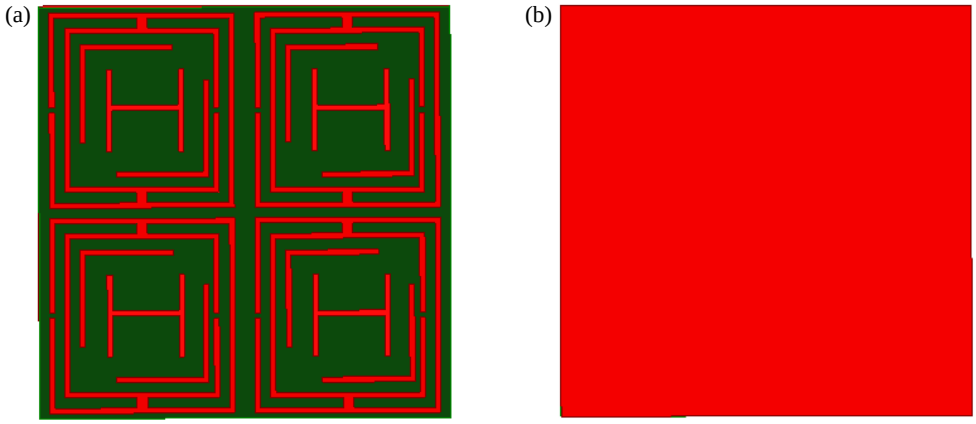

FIGURE 11. 2×2 H-shaped MMA. (a) Top surface. (b) Bottom surface.

6.2. 4×4 Array

To estimate MMA efficiency, unit-cell analysis is insufficient, and an array analysis is important. Several applications utilize arrays; therefore, the performance of a 4×4 array is analyzed using a simulation setup similar to that of an H-shaped unit cell. By utilizing the 4×4 array periodicity of the unit cell, the proposed design can perform more accurately. The fabricated prototype and the measurement equipment are shown in Figures 14 and 15, respectively. Array analysis was performed by applying appropriate boundary conditions and utilizing a Floquet port to excite the structure. The simulation of the 4×4 array was carried out by considering the frequency domain and by selecting the field monitors at 3.17 GHz to capture the necessary field distributions. The S-parameters were evaluated by monitoring the S-parameters particularly S_{11} and S_{21} to analyse the reflective and cross-polarized responses. These parameters are essential for evaluating the behavior of a metasurface for S-band and satellite communication applications. The reflection coefficient of the 4×4 H-shaped MMA is shown in Figure 16. S_{11} of -32 dB has been observed at 3.17 GHz and 7.78 GHz. It provides dual absorption bandwidths of 710 MHz and 1630 MHz with FBWs of 22.95% and 19.35% respectively.

7. POLARIZATION INSENSITIVITY ANALYSIS OF THE H-SHAPED MMA

By examining the impacts of the incidence and polarization angles, the polarization independent features of the suggested MMA are examined in this section. The polarization insensitivity analysis of the H-shaped MMA, by varying the incidence angle (θ) from 0° to 90°, is shown in Figure 17 with the H-field in the Y-axis and the E-field in the X-axis. Both normal and oblique incidence electromagnetic waves exhibit polarization insensitivity. The H-shaped MTM unit cell is independent of the polarizing angle owing to its unique properties. Figure 17(a) shows that changing "θ" from 0° to 90° resulted in the same absorption. The H-shaped MTM unit cell was demonstrated to be independent of polarization. An analysis was performed on how "θ" and "Φ" affect the absorptivity under TM and TE polarizations. As illustrated in Figure 17(b), the polarization angle is varied between 0° and 90° while the H-field remains constant.

$$\Gamma(\omega) = \frac{Z(\omega)\cos\theta - Z_0\cos\theta'}{Z(\omega)\cos\theta + Z_0\cos\theta'} \tag{10}$$

where θ and θ' are incident and transmission angles, respectively. Because of its distinct design geometry, the suggested

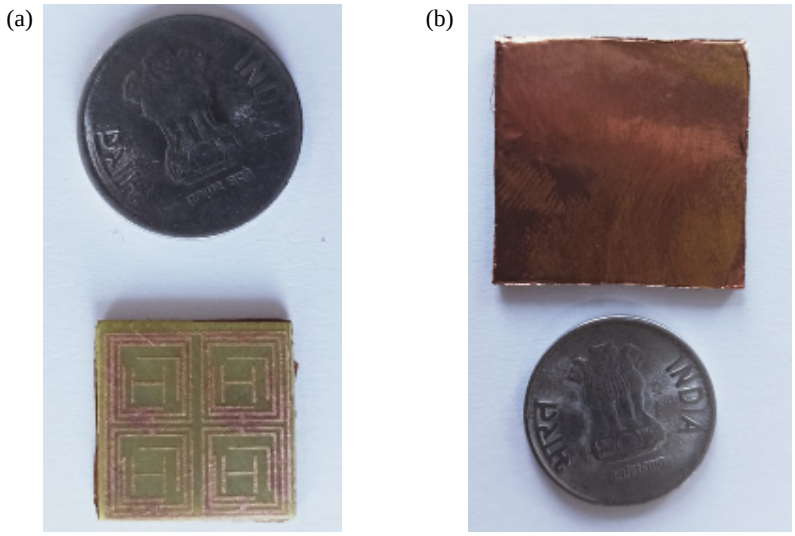

FIGURE 12. Prototype of 2 × 2 H-shaped MMA. (a) Top surface. (b) Bottom surface.

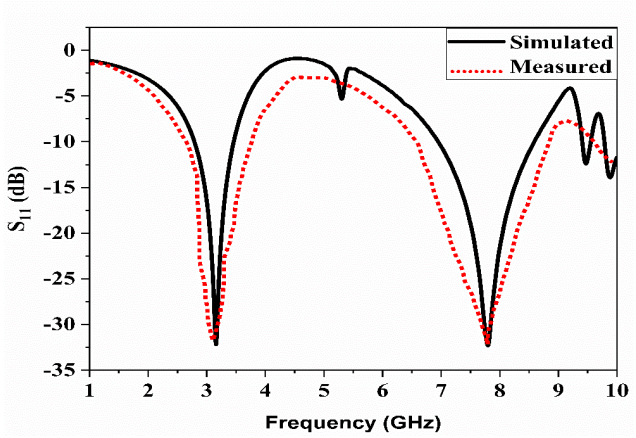

FIGURE 13. Reflection coefficient of the 2 × 2 H-shaped MMA.

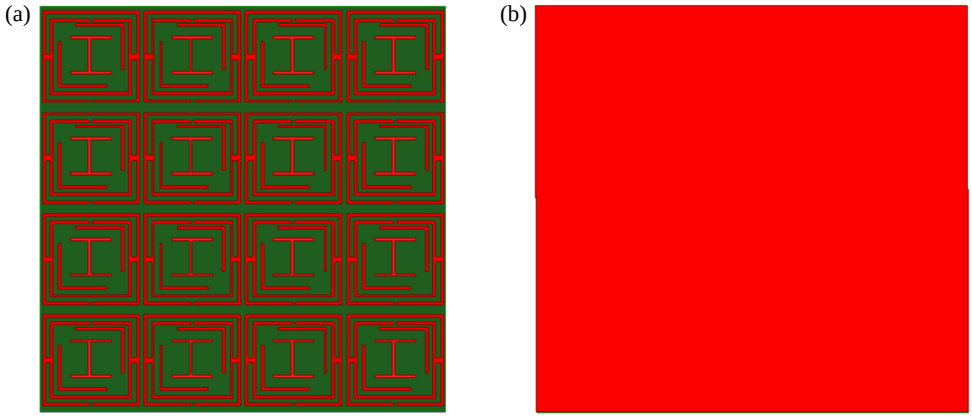

FIGURE 14. 4 × 4 H-shaped MMA. (a) Top view. (b) Bottom view.

structure is therefore independent of all polarizing angles. The suggested MTM structure may be a viable choice for S-band and satellite communication applications due to its constant response across all incident angles. This research explores the polarization stability of the proposed unit cell configuration via transverse electric (TE) and transverse magnetic (TM) analysis, as shown in Figures 17(a) and 17(b). The structure is subjected to simulation under normal incidence conditions. Figures 17(a) and 17(b) illustrate the simulated absorption for various oblique incidence angles corresponding to transverse electric (TE) and transverse magnetic (TM) polarized incidence waves, respectively. Moreover, owing to the geometric configuration and

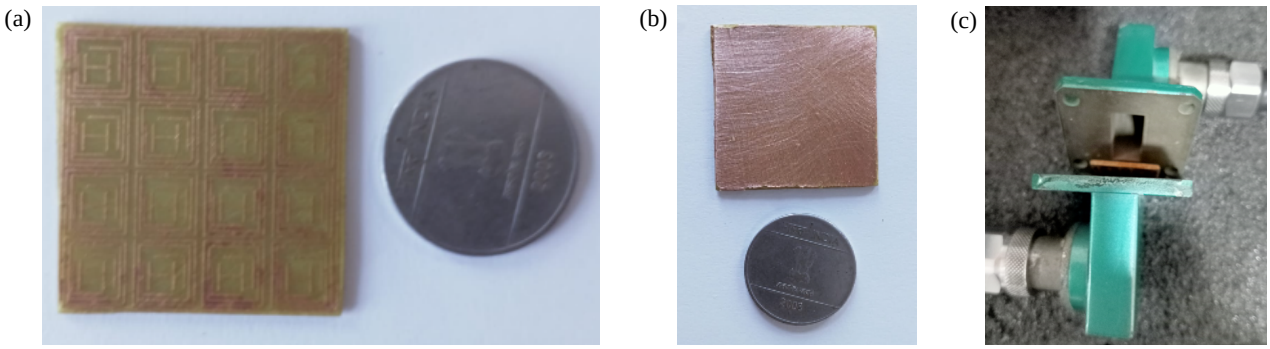

FIGURE 15. Prototype of the 4×4 H-shaped MMA.

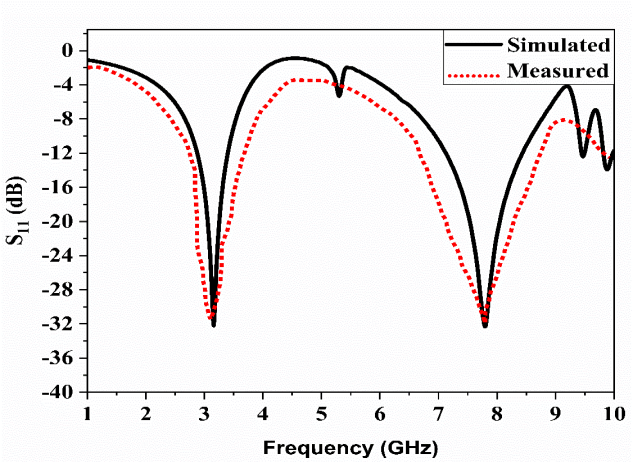

FIGURE 16. Reflection coefficient of the 4×4 H-shaped MMA.

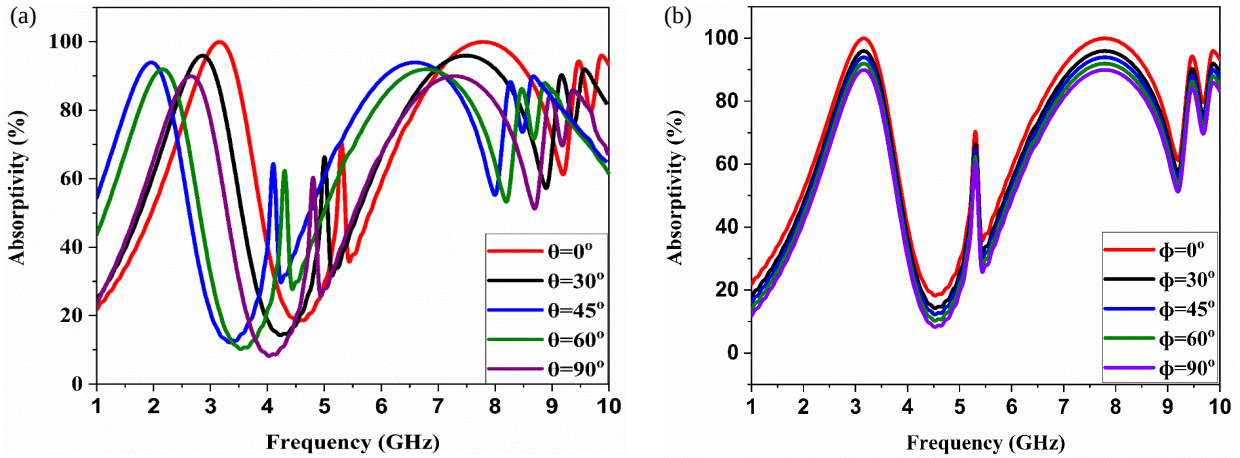

FIGURE 17. Absorptivity (%) response of the proposed H-shaped MMA for different (a) θ°, (b) Φ°.

symmetry, both TE and TM polarizations exhibit significant angular stability. For TE polarization, incidence angles of 0°, 30°, 45°, 60° and 90° yield absorption exceeding 90% across the frequency band, as demonstrated in Figure 17(a).

Additionally, the bandwidth ratio approaches unity for both bands, signifying enhanced angular stability. Figure 17(b) presents the absorption curve for TM polarization. When an electromagnetic wave strikes on the metasurface absorber at an oblique incidence angle of 90°, the TE and TM modes reveal unique responses attributable to the engagement of the electric (E) and magnetic (H) fields with the surface configuration, as represented in Figure 17(b). Polarization sensitivity of a metasurface means that its response absorption changes depending on the wave's polarization. A polarization-sensitive design behaves the same for any polarization. A sensitive design behaves differently for TE vs TM. TE and TM simulations for 0°, 30°, 45°, 60°, and 90° incidence are shown in Figure 17(a) and (b).

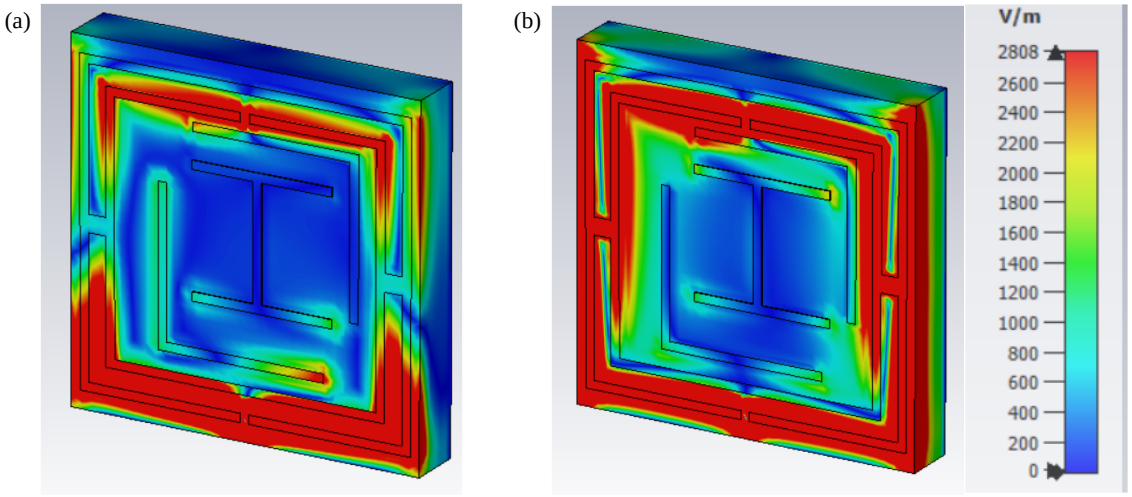

FIGURE 18. E-field distribution of the H-shaped absorber: (a) 3.17 GHz (b) 7.78 GHz.

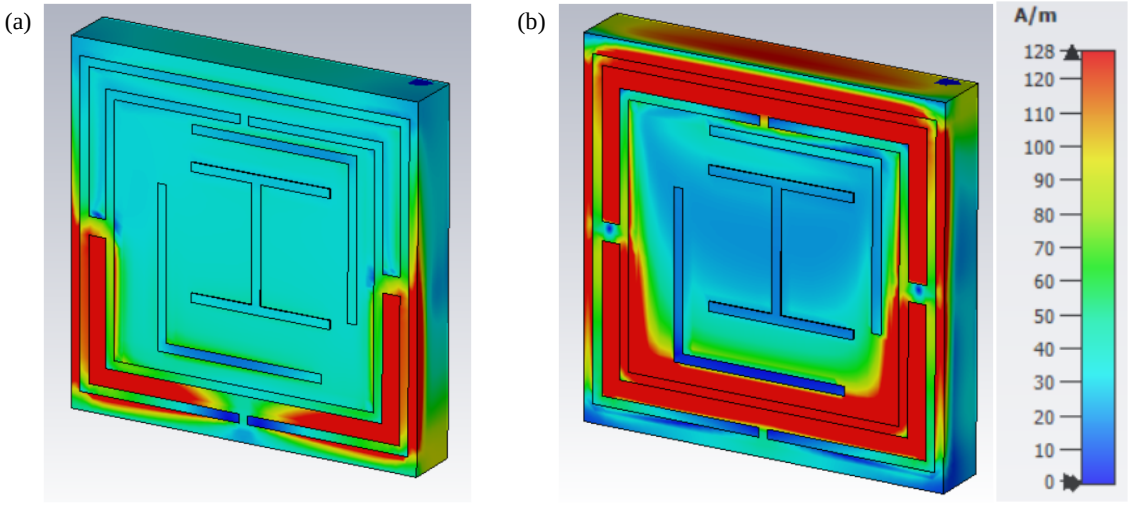

FIGURE 19. H-field distribution of the H-shaped absorber: (a) 3.17 GHz (b) 7.78 GHz.

8. ELECTRIC (E), MAGNETIC (H) FIELDS AND SURFACE CURRENT DISTRIBUTIONS ANALYSIS

The working mechanism of the MMA has been explained by analysing its E and H-fields, as well as its surface current distributions. Figure 18 demonstrates the distribution schematics of E-fields at 3.17 GHz and 7.78 GHz. At 3.17 GHz, the maximum distribution is visualized at the pair of SRRs [Figure 18(a)]. At 7.78 GHz, the E-field intensity is highly visible at the corners of the structure, whereas a relatively lower intensity is observed in the central portions of the geometry, as depicted in Figure 18(b). Figure 19 shows the magnetic (H) field distributions at the same frequencies (3.17, 7.78 GHz). Figure 19(a) shows that the magnetic field intensity increases near the lower half of the SRRs for 3.17 GHz. According to Figure 19(b), at 7.78 GHz, a high level of H-field intensity is observed around all sides of the MMA unit cell, as marked by the red-coloured region. However, the H-field intensity is significantly lower near the central portion of the absorber model. Similarly, the performance of the MMA is investigated by analysing surface current (J-surf) distributions at 3.17 GHz and 7.78 GHz. Figure 20 shows that the split ring and H-shaped configurations are the primary locations for surface current. The maximum distribution is represented by using red color, and vice versa. The maximum amount of field is concentrated on the ends of split rings, as well as on the H-shaped resonator of the unit cell.

9. COMPARATIVE ANALYSIS OF THE PERFORMANCE PARAMETERS WITH THE STATE OF THE ART

Table 1 presents a performance comparison table, summarizing a comparative analysis of the proposed MMA with other previously reported absorbers [8–30]. The complete analysis was performed by considering the crucial parameters, such as electrical dimensions and size of the unit cell, and EM performance parameters, such as polarization insensitivity, absorption efficiency, and angular stability. Several designs obtain an absorption value of 0.9, indicating that EM energy is ab-

TABLE 1. H-shaped MTM absorber (MMA) comparison with some of the previously reported absorbers from the literature.

Ref.	Unit Cell Size (mm^2)	Electrical Size (mm^2)	Substrate	Resonating Band	Angular Stability	Absorption	Polarization Insensitivity
[8]	10×10	$0.33\lambda \times 0.33\lambda$	FR4	S/X	NA	NA	No
[11]	5×5	$0.161\lambda \times 0.161\lambda$	FR4	C	NA	NA	No
[16]	12×12	$0.134\lambda \times 0.134\lambda$	FR4	S/C/X	NA	NA	No
[17]	6×6	$0.086\lambda \times 0.086\lambda$	FR4	C/X	NA	NA	No
[18]	9×8.8	$0.125\lambda \times 0.125\lambda$	FR4	X/Ku	NA	NA	No
[19]	5×5	$0.232\lambda \times 0.232\lambda$	FR4	Ku/K	NA	NA	No
[20]	10×10	$0.26\lambda \times 0.26\lambda$	FR4	C/X/Ku	NA	NA	No
[21]	10×8	$0.29\lambda \times 0.24\lambda$	FR4	X	NA	NA	No
[22]	8×8	$0.15\lambda \times 0.15\lambda$	FR4	C	NA	NA	No
[23]	10×10	$0.252\lambda \times 0.252\lambda$	FR4	C, X	NA	NA	No
[24]	7.6×7.6	$2\lambda \times 2\lambda$	FR4	C/X	0–50°	91	Yes
[25]	10×10	$0.18\lambda \times 0.18\lambda$	FR4	S/C	0–60°	85	Yes
[26]	5×5	$0.232\lambda \times 0.232\lambda$	FR4	Ku/K	NA	NA	No
[27]	10×10	$0.116\lambda \times 0.116\lambda$	FR4	S/C	0–60°	97	No
[28]	8×8	$0.15\lambda \times 0.15\lambda$	Rogers RT5870	C/X	0–60°	97	No
[29]	10×10	$0.147\lambda \times 0.147\lambda$	FR4	S/C/X and Ku	0–90°	97	No
[30]	16×28.5	$0.353\lambda \times 0.412\lambda$	FR4	L/S	0–90°	95	No
This Work	10×10	$0.09\lambda \times 0.09\lambda$	FR4	S/C	0–90°	99.99	Yes

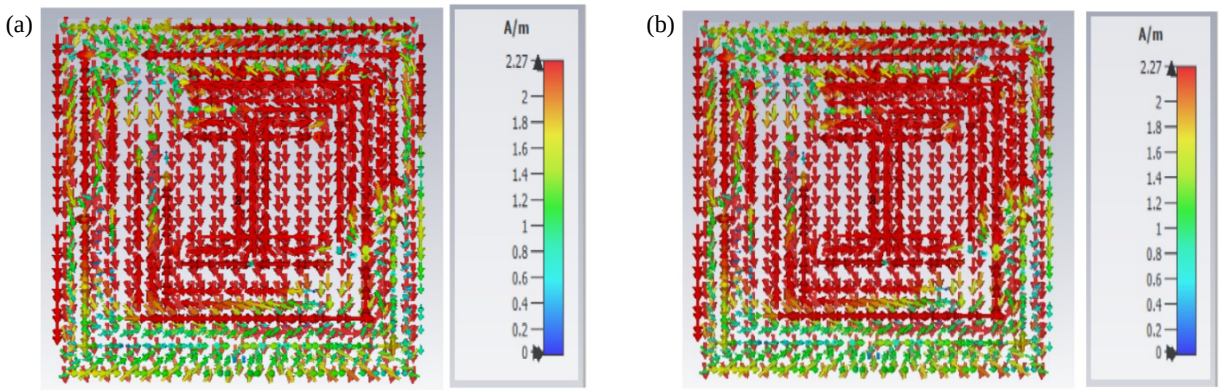

FIGURE 20. Surface distribution at (a) 3.17 GHz and (b) 7.78 GHz.

sorbed. In real-time applications, the most important parameter is polarization insensitivity; none of the studies listed provided up to 90° polarization insensitivity. When designing high-efficiency absorbers, a compromise between various performance parameters and substrate selection is crucial. Furthermore, the above-mentioned absorbers offer less absorption with no polarization insensitivity. In addition to that the size of the absorber is smaller than that [11, 17–20, 22, 24, 26, 28], and polarization insensitivity has not been provided up to 900. Though [8, 20, 23, 25, 27, 29] occupy the same size as that of the proposed absorber, it does not provide angular stability (or) polarization insensitivity. Despite exhibiting an absorption of more than 90%, [8–30] fails to deliver angular stability up to 90°. Although Ref. [25] covers the S and C bands and occupies $10 \times 10\,mm^2$ dimensions, polarization sensitivity has been shown up to 60°. Ref. [30] takes up more space than the intended absorber, and it does not possess a polarization-insensitive nature. Even though Refs. [27, 29] have the same size as the suggested absorber, they do not report angular stability and polarization sensitivity features. Finally, it can be summarized that the suggested H-shaped metamaterial-based absorber is capable of absorbing dual bands of 710 GHz and 1630 GHz, with polarization-insensitivity up to 90°, and shows 99.99% peak absorption of the signal.

In conclusion, the H-shaped metamaterial-based absorber offers wide bandwidths of 0.7 GHz and 1.5 GHz and shows polarization insensitivity up to 90°, with an absorption of 99.99%. These results indicate that the proposed absorber is suitable for both S-band and satellite communication applications.

10. CONCLUSIONS

A dual-band polarization-insensitive compact metamaterial absorber is introduced for satellite communication applications. The recommended H-shaped resonator-based MMA is compact and easy to design. The H-shaped MTM absorber has dual absorption bandwidths of 710 MHz (2.74 GHz–3.45 GHz) and 1630 MHz (6.95 GHz–8.58 GHz) with FBWs of 22.95% and 19.35 %, considering more than 90% absorption at wide range. The MTM unit cell occupies an area of $0.09\lambda \times 0.09\lambda$ with a thickness of 0.145λ. The proposed polarization-insensitive MMA exhibits stability when using oblique incident waves. For the TE and TM waves, the absorption level was outstanding at all the incidence and polarization angles. A parametric analysis was conducted on several geometric factors, including the length and width of the H-shaped resonators, to attain the required absorption rates for a dual-band spectrum within a compact size. The structure has the following benefits: high absorption, wide bandwidth, ultra-fast response time, simplicity of construction, and polarization insensitivity.

REFERENCES

[1] Haque, S. M. A., M. T. Islam, A. G. Alharbi, A. Miah, S. A. Zafir, and M. Samsuzzaman, "Double stripe square enclosed SRR based triple band metamaterial absorber for materials variation and thickness sensing applications," *Optics Communications*, Vol. 583, 131740, 2025.

[2] Hannan, S., M. T. Islam, M. R. I. Faruque, and H. Rmili, "Polarization-independent perfect metamaterial absorber for C, X and, Ku band applications," *Journal of Materials Research and Technology*, Vol. 15, 3722–3732, 2021.

[3] Amiri, M., F. Tofigh, N. Shariati, J. Lipman, and M. Abolhasan, "Wide-angle metamaterial absorber with highly insensitive absorption for TE and TM modes," *Scientific Reports*, Vol. 10, No. 1, 13638, 2020.

[4] Islam, M. T., M. R. Islam, M. T. Islam, A. Hoque, and M. Samsuzzaman, "Linear regression of sensitivity for meander line parasitic resonator based on ENG metamaterial in the application of sensing," *Journal of Materials Research and Technology*, Vol. 10, 1103–1121, 2021.

[5] Alexandropoulos, G. C., G. Lerosey, M. Debbah, and M. Fink, "Reconfigurable intelligent surfaces and metamaterials: The potential of wave propagation control for 6G wireless communications," *arXiv Preprint arXiv:2006.11136*, 2020.

[6] Zhang, Y., Z. Yi, X. Wang, P. Chu, W. Yao, Z. Zhou, S. Cheng, Z. Liu, P. Wu, M. Pan, and Y. Yi, "Dual band visible metamaterial absorbers based on four identical ring patches," *Physica E: Low-dimensional Systems and Nanostructures*, Vol. 127, 114526, 2021.

[7] Islam, M. R., M. Samsuzzaman, N. Misran, G. K. Beng, and M. T. Islam, "A tri-band left-handed meta-atom enabled designed with high effective medium ratio for microwave based applications," *Results in Physics*, Vol. 17, 103032, 2020.

[8] Islam, M. S., M. Samsuzzaman, G. K. Beng, N. Misran, N. Amin, and M. T. Islam, "A gap coupled hexagonal split ring resonator based metamaterial for S-band and X-band microwave applications," *IEEE Access*, Vol. 8, 68 239–68 253, 2020.

[9] Moniruzzaman, M., M. T. Islam, M. T. Islam, M. E. H. Chowdhury, H. Rmili, and M. Samsuzzaman, "Cross coupled interlinked split ring resonator based epsilon negative metamaterial with high effective medium ratio for multiband satellite and radar communications," *Results in Physics*, Vol. 18, 103296, 2020.

[10] Shah, S. M. Q. A., N. Shoaib, F. Ahmed, A. Alomainy, A. Quddious, S. Nikolaou, M. A. Imran, and Q. H. Abbasi, "A multiband circular polarization selective metasurface for microwave applications," *Scientific Reports*, Vol. 11, No. 1, 1774, 2021.

[11] Almutairi, A. F., M. S. Islam, M. Samsuzzaman, M. T. Islam, N. Misran, and M. T. Islam, "A complementary split ring resonator based metamaterial with effective medium ratio for C-band microwave applications," *Results in Physics*, Vol. 15, 102675, 2019.

[12] Islam, M. S., M. T. Islam, N. M. Sahar, H. Rmili, N. Amin, and M. E. H. Chowdhury, "A mutual coupled concentric crossed-Line split ring resonator (CCSRR) based epsilon negative (ENG) metamaterial for tri-band microwave applications," *Results in Physics*, Vol. 18, 103292, 2020.

[13] Moniruzzaman, M., M. T. Islam, G. Muhammad, M. S. J. Singh, and M. Samsuzzaman, "Quad band metamaterial absorber based on asymmetric circular split ring resonator for multiband microwave applications," *Results in Physics*, Vol. 19, 103467, 2020.

[14] Srinivasan, K., N. B. Ali, Y. Trabelsi, M. S. M. Rajan, and M. Kanzari, "Design of a modified single-negative metamaterial structure for sensing application," *Optik*, Vol. 180, 924–931, 2019.

[15] Moniruzzaman, M., M. T. Islam, N. Misran, M. Samsuzzaman, T. Alam, and M. E. H. Chowdhury, "Inductively tuned modified split ring resonator based quad band epsilon negative (ENG) with near zero index (NZI) metamaterial for multiband antenna performance enhancement," *Scientific Reports*, Vol. 11, No. 1, 11950, 2021.

[16] Hossain, M. J., M. R. I. Faruque, and M. T. Islam, "Design and analysis of a new composite double negative metamaterial for multi-band communication," *Current Applied Physics*, Vol. 17, No. 7, 931–939, 2017.

[17] Marathe, D. and K. Kulat, "A compact triple-band negative permittivity metamaterial for C, X-band applications," *International Journal of Antennas and Propagation*, Vol. 2017, No. 1, 7515264, 2017.

[18] Hossain, T. M., M. F. Jamlos, M. A. Jamlos, P. J. Soh, M. I. Islam, and R. Khan, "Modified H-shaped DNG metamaterial for multiband microwave application," *Applied Physics A*, Vol. 124, No. 2, 183, 2018.

[19] Azeez, A. R., T. A. Elwi, and Z. A. A. AL-Hussain, "Design and analysis of a novel concentric rings based crossed lines single negative metamaterial structure," *Engineering Science and Technology, an International Journal*, Vol. 20, No. 3, 1140–1146, 2017.

[20] Tamim, A. M., M. R. I. Faruque, M. J. Alam, S. S. Islam, and M. T. Islam, "Split ring resonator loaded horizontally inverse double L-shaped metamaterial for C-, X-and Ku-band microwave applications," *Results in Physics*, Vol. 12, 2112–2122, 2019.

[21] Ahamed, E., M. R. I. Faruque, M. F. B. Mansor, and M. T. Islam, "Polarization-dependent tunneled metamaterial structure with enhanced fields properties for X-band application," *Results*

in Physics, Vol. 15, 102530, 2019.

[22] Ramachandran, T., M. R. I. Faruque, and M. T. Islam, "A dual band left-handed metamaterial-enabled design for satellite applications," *Results in Physics*, Vol. 16, 102942, 2020.

[23] Hasan, M. M., M. R. I. Faruque, S. S. Islam, and M. T. Islam, "A new compact double-negative miniaturized metamaterial for wideband operation," *Materials*, Vol. 9, No. 10, 830, 2016.

[24] Chen, X., T. M. Grzegorczyk, B.-I. Wu, J. Pacheco, and J. A. Kong, "Robust method to retrieve the constitutive effective parameters of metamaterials," *Physical Review E*, Vol. 70, 016608, 2004.

[25] Sabah, C. and T. Nesimoglu, "Design and characterization of a resonator-based metamaterial and its sensor application using microstrip technology," *Optical Engineering*, Vol. 55, No. 2, 027107, 2016.

[26] Afsar, M. S. U., M. R. I. Faruque, S. Abdullah, and K. S. Al-Mugren, "Compact and polarization insensitive satellite band perfect metamaterial absorber for effective electromagnetic communication system," *Materials*, Vol. 16, No. 13, 4776, 2023.

[27] Jahan, M. I., M. R. I. Faruque, M. B. Hossain, M. U. Khandaker, F. Elsayed, M. Salman, and H. Osman, "Quad-band metamaterial perfect absorber with high shielding effectiveness using double X-shaped ring resonator," *Materials*, Vol. 16, No. 12, 4405, 2023.

[28] Ranjan, S. K. and S. Sahoo, "Hexagon enclosed modified G-shaped polarization and incident angle independent metamaterial absorber for S, C, X and Ku band frequency," *AEU — International Journal of Electronics and Communications*, Vol. 183, 155348, 2024.

[29] Bhupathi, A. K., R. Yarlagadda, and M. P. Avala, "Design and characterization of an earbud-shaped wideband metamaterial absorber for electronic warfare," *Proceedings of the Indian National Science Academy*, 1–10, 2025.

[30] Moniruzzaman, M., S. Larguech, M. Mobarak, N. M. Jizat, S. S. Alharbi, M. T. Islam, M. Samsuzzaman, and S. S. Al-Bawri, "Dual band polarization insensitive metamaterial absorber for EMI shielding from GSM and 5G communication systems," *Scientific Reports*, Vol. 15, 12292, 2025.

[31] Valathuru, M., P. Pardhasaradhi, N. Prasad, B. T. P. Madhav, S. Das, N. F. Soliman, and M. E. Ghzaoui, "Design and analysis of dual-band hexagon-shaped polarization-insensitive metamaterial absorber using vanadium dioxide (VO_2) for terahertz applications," *Plasmonics*, Vol. 20, No. 6, 4221–4240, 2025.

[32] Valathuru, M., P. Pardhasaradhi, N. Prasad, B. T. P. Madhav, S. Das, A. D. Algarni, and M. E. Ghzaoui, "Design and analysis of metamaterial-based ultra-broadband micro-scaled absorber with vanadium dioxide (VO_2) and silicon dioxide (SiO_2) for multiple terahertz applications," *Photonics and Nanostructures — Fundamentals and Applications*, Vol. 64, 101381, 2025.

[33] Prasad, N., P. Pardhasaradhi, B. T. P. Madhav, J. L. Narayana, T. Islam, M. E. Ghzaoui, and S. Das, "Quartz substrate-based super absorber using graphene material with 18 absorption bands for terahertz applications," *Plasmonics*, Vol. 20, No. 4, 1921–1933, 2025.

[34] Prasad, N., B. T. P. Madhav, N. A. Murugan, S. Das, T. Altameem, and W. El-Shafai, "A metamaterial broadband absorber by tuning single graphene material for various terahertz domain applications," *Diamond and Related Materials*, Vol. 150, 111705, 2024.

[35] Rekha, V. S. D., N. Prasad, B. T. P. Madhav, and M. Alathbah, "Design and analysis of minkowski fractal shaped metasurface absorber with broadband and polarization-insensitive characteristics using a tunable graphene layer for terahertz applications," *Physica Scripta*, Vol. 99, No. 8, 085934, 2024.